Results in Applied Mathematics 8 (2020) 100110

Contents lists available at ScienceDirect

Results in Applied Mathematics

journal homepage: www.elsevier.com/locate/results-in-applied-mathematics

Interface Flux Recovery coupling method for the ocean–atmosphere system

K. Chad Sockwell [*,1], Kara Peterson [1], Paul Kuberry [1], Pavel Bochev [1], Nat Trask [1]

Center for Computing Research, Sandia National Laboratories, MS-1320, Albuquerque, NM 87185-1320, USA

ARTICLE INFO

Article history:
Received 2 January 2020
Received in revised form 29 March 2020
Accepted 22 April 2020
Available online 16 May 2020

Keywords:
Ocean–atmosphere coupling
Flux recovery
Coupling methods
Schur complement
Monolithic formulation

ABSTRACT

Component coupling is a crucial part of climate models, such as DOE's E3SM (Caldwell et al., 2019). A common coupling strategy in climate models is for their components to exchange flux data from the previous time-step. This approach effectively performs a single step of an iterative solution method for the monolithic coupled system, which may lead to instabilities and loss of accuracy. In this paper we formulate an Interface-Flux-Recovery (IFR) coupling method which improves upon the conventional coupling techniques in climate models. IFR starts from a monolithic formulation of the coupled discrete problem and then uses a Schur complement to obtain an accurate approximation of the flux across the interface between the model components. This decouples the individual components and allows one to solve them independently by using schemes that are optimized for each component. To demonstrate the feasibility of the method, we apply IFR to a simplified ocean–atmosphere model for heat-exchange coupled through the so-called bulk condition, common in ocean–atmosphere systems. We then solve this model on matching and non-matching grids to estimate numerically the convergence rates of the IFR coupling scheme.

1. Introduction

Efficient, accurate, and stable coupling schemes, or couplers, are essential for large scale predictive simulations of complex multiphysics phenomena such as the global earth system; see [1]. Efficiency can be achieved by designing the coupler in such a way that each constituent component of the model can be discretized and solved independently from the other components. Most couplers accomplish this by lagging the coupling condition at the previous time-step, thus allowing each component to run autonomously in between coupling steps.

This so-called loosely coupled, or partitioned, methodology [2,3] is minimally intrusive, which allows each component of the multi-physics models to be built, optimized, and evaluated separately from the other components. Effectively, every component is treated as a black box by all other components. This allows for greater flexibility and speed of development in multi-physics codes such as E3SM [1]. However, mathematically such couplers can be viewed as performing a single step of an iterative solution procedure for the fully coupled monolithic system. As a result, they are prone to instabilities [4]

* Corresponding author.
E-mail addresses: kcsockw@sandia.gov (K.C. Sockwell), kjpeter@sandia.gov (K. Peterson), pakuber@sandia.gov (P. Kuberry), pbboche@sandia.gov (P. Bochev), natrask@sandia.gov (N. Trask).

[1] Sandia National Laboratories is a multimission laboratory managed and operated by National Technology and Engineering Solutions of Sandia, LLC., a wholly owned subsidiary of Honeywell International, Inc., for the U.S. Department of Energy's National Nuclear Security Administration under contract DE-NA-0003525. This paper describes objective technical results and analysis. Any subjective views or opinions that might be expressed in the paper do not necessarily represent the views of the U.S. Department of Energy or the United States Government.

https://doi.org/10.1016/j.rinam.2020.100110

and may require additional mechanisms such as Anderson acceleration [5], or modified transmission conditions [6] to ensure acceptable accuracy and/or stability.

Many of these issues can be avoided by treating the constituent model components as *gray* instead of as black boxes. Black box components typically provide information only about their field values on the interface. In contrast, a gray box component can also be queried about *additional interface entities* such as the element stiffness and mass matrices along the interface. This additional information can significantly improve the accuracy of, e.g., the fluxes exchanged by the components. For example, if two black box components exchange finite element field values, the interface flux is usually computed by differentiating these finite element fields, leading to the loss of one order of accuracy. In contrast, a gray box coupler would provide enough information to perform a more accurate variational flux recovery [7], which provides an optimally accurate flux approximation.

In this paper we refer to couplers employing black box components as *agnostic*, whereas couplers that employ gray boxes are termed *informed*. Another example of an informed strategy would be to make the coupler aware of the monolithic structure of the coupled model. Depending on this structure, the coupler may be able to find the flux in the monolithic model at the current time-step, without having to solve it. The implicit value recovery (IVR) method implements this type of strategy [8] for monolithic models whose semi-discrete in space formulations can be reduced to Hessenberg index-1 Differential Algebraic Equations (DAEs).

For the informed coupling scheme to retain the advantages of the agnostic coupling scheme, it must still be non-intrusive to each component that it couples and allow these components to run in a decoupled manner. This means the coupler must not demand significant structural changes in the codes implementing the components, nor solve for the components in a tightly coupled manner. At the same time, the informed scheme must be able to query information about the model equations, which is possible with today's modular software construction. In the worse case scenario where this information is not available, the coupler must produce the information. The IVR method follows this paradigm of well-informed but non-intrusive coupling. In this work, we draw upon the ideas of IVR to develop an informed coupler for a representative coupling problem in Earth System Models. Specifically, we focus on the heat exchange in the ocean–atmosphere system connected by a Robin-like transmission condition known as the "bulk condition".

Coupled climate models, or more simply, coupled climate systems such as the ocean–atmosphere system are a taxing application for any coupler. Climate models require fine resolution and long time-horizons to make meaningful predictions. They also possess multi-scale behavior which further complicates the coupling process. As a result, the climate system requires a coupling scheme which is stable for long time horizons, conservative, and sufficiently accurate. In this paper we will limit our concern to the largest coupled system in the Earth system, the ocean–atmosphere system. We chose this system for several reasons. First, it comprises the two largest components in the climate system, both possessing multiple time-scales. Second, the ocean–atmosphere system has been studied by both domain experts [9–11] and mathematicians [12–16] alike, resulting in a better understanding of its properties relative to the other subsystems in the Earth System Model. Finally, the bulk coupling conditions in this subsystem are similar in nature to those which exist between other pairs of components in the climate system.

The stability of various agnostic coupling schemes for the bulk condition applied to the heat equation is investigated in [17] for implicit time-stepping methods. Similar analysis of agnostic couplers for the more general ocean–atmosphere system is carried out in [15,16,18,19]. Collectively, it has been shown that most such couplers are either unconditionally stable or conserve flux. This fact motivates our interest in alternative informed coupling strategies for the bulk condition as a potential pathway towards couplers that are both conservative and unconditionally stable, while still allowing for a decoupled solution of the component models.

This work is a first step in that direction in which we extend the IVR coupler to a *Bulk-Interface-Flux-Recovery* (Bulk-IFR) coupler designed for the bulk condition case. The IVR approach was formulated for "perfect" transmission conditions [20] which enforce both *continuity of a quantity and its flux* across the interface. In contrast, the bulk coupling condition [12–14] in the ocean–atmosphere system is derived through drag laws on the interface and states that the flux of a quantity through the interface is proportional to the jump of that quantity across the interface, i.e., it is an example of an "imperfect" coupling condition.

This makes the Bulk-IFR extension presented in this paper different from its IVR parent in a non-trivial way. IVR starts from a semi-discrete in space monolithic formulation, in which the perfect coupling condition is enforced by a Lagrange multiplier, and which is a Hessenberg index-2 DAE. Differentiation of the constraint equation in time reduces the index to one; application of explicit time stepping to this DAE then effectively decouples its components.

In contrast, IFR treats the bulk coupling condition as an independent interface equation and introduces the interface flux as a new dependent variable. Discretization in space then leads to a monolithic problem in which the states and the flux are coupled through the interface equation, which prevents us from applying the time differentiation "trick" from IVR to that equation. Instead, we proceed to discretize in time and formulate the Bulk-IFR coupler for the fully discrete monolithic problem. The structure of this problem allows us to decouple its components by solving a Schur complement equation for the dependent flux variable, as in the IVR scheme. After solving this equation the flux is treated as a boundary condition by the two subsystems at the next time-step.

Because the Schur complement is formed for the fully discrete monolithic problem Bulk-IFR is not limited to the explicit time integration schemes required to perform the decoupling in IVR. Another important distinction stems from the fact that the bulk condition couples the states and the flux variable. As a result, the structure of the fully discrete monolithic

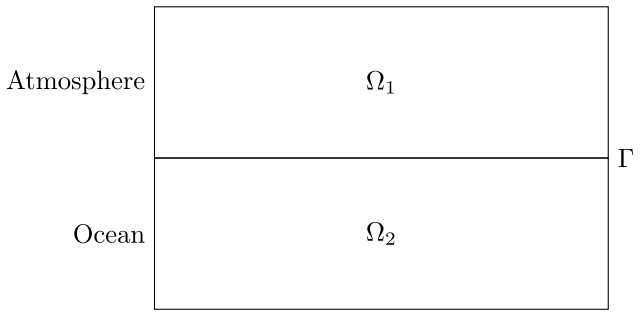

Fig. 1. Ocean-atmosphere domain with interface Γ.

problem in the Bulk-IFR coupler resembles that of *stabilized mixed variational problems* [21], which are not subject to an inf–sup stability condition [22]. In contrast, the monolithic problem in the IVR coupler is of the *mixed type* [23,24], which implies an inf–sup condition, which must be satisfied. Consequently, the IFR coupler allows for a greater flexibility in the discretization of the flux variable than the IVR coupler.

Although the new Bulk-IFR method leads to fully decoupled sub-problems, solution of the Schur complement still recovers the exact flux of the discretized monolithic system. As a result, the Bulk-IFR scheme does not introduce any of the partitioning errors that are pervasive in most agnostic couplers. We note that the scope of the Bulk-IFR coupler extends to any coupled problem with a Robin-like "imperfect" transmission condition.

The layout of the paper is as follows. In Section 2, we describe the simple heat transfer model for the ocean–atmosphere system. The Bulk-IFR scheme is described for the model in Section 3. The scheme is derived for both implicit and explicit time-stepping schemes. However, demonstration of the method to implicit and hybrid implicit–explicit time-stepping schemes is beyond the scope of this work and will be reported in a forthcoming paper. The simplified test case, representative of the heat transfer in the ocean–atmosphere system is described in Section 4. Finally the Bulk-IFR method is applied to the test case with explicit time stepping and convergence rates are shown for matching grids and non-matching grids for each domain. In this work, we only aim to simply extend the IVR method to the bulk condition case, and reserve further analysis for future research.

2. Governing equations

As a simplified proxy for a coupled ocean/atmosphere system we consider a specialized form of the advection–diffusion equation on two subdomains $\Omega_1, \Omega_2 \in \mathbb{R}^2$, with boundaries $\partial\Omega_1$ and $\partial\Omega_2$, separated by a common one-dimensional interface Γ. The two subdomains are stacked vertically and the governing equations are defined so that diffusion occurs in the vertical (y) direction and advection in the horizontal (x) direction. The governing equations can then be written as

$$\frac{\partial \varphi_i}{\partial t} - \frac{\partial}{\partial y} k_i \frac{\partial \varphi_i}{\partial y} + u_i \frac{\partial \varphi_i}{\partial x} = f_i \quad \text{in } \Omega_i \times [0, T] \quad i = 1, 2\,, \tag{2.1}$$

with initial conditions

$$\varphi_i(x, y, 0) = \varphi_i^0(x, y) \quad \text{in } \Omega_i \quad i = 1, 2\,, \tag{2.2}$$

and boundary conditions

$$\varphi_i = g_i \quad \text{on } \partial\Omega_i \setminus \Gamma \quad i = 1, 2\,. \tag{2.3}$$

These two sets of equations are connected through a bulk interface condition stating that the flux between the two subdomains is continuous and equal to a function of the jump in the solution. Succinctly,

$$k_1 \frac{\partial \varphi_1}{\partial y} \hat{y} \cdot \hat{n} = k_2 \frac{\partial \varphi_2}{\partial y} \hat{y} \cdot \hat{n} = \alpha(\varphi_1 - \varphi_2) \quad \text{on } \Gamma\,, \tag{2.4}$$

where $\hat{y}$ is the unit vector in the y direction and $\hat{n}$ is a specified normal direction perpendicular to the interface. We will choose a simple rectangular domain, partitioned across the y direction so that $\hat{n}$ is parallel or anti-parallel to $\hat{y}$. A simple schematic of the domain is given in Fig. 1. We adopt the convention that the unit normal vectors $\hat{n}_1$ and $\hat{n}_2$ for Ω_1 and Ω_2, respectively point outward from the respective domain. Based on the schematic and choosing upward to be the positive y direction, we will choose $\hat{n} = \hat{n}_2$ pointing in the positive y direction. This is very natural since we think of the atmosphere being above the ocean. Therefore we will have a change of sign in the boundary condition for the equation in Ω_1.

To derive the Bulk-IFR scheme we begin with monolithic formulation of the model problem obtained by introducing the interface flux as a new dependent variable λ and adding a weak form of the bulk condition (2.4) to the weak

forms of the differential equations in (2.1). The resulting monolithic weak problem is given by; seek $\{\varphi_1, \varphi_2, \lambda\} \in H^1_D(\Omega_1) \times H^1_D(\Omega_2) \times H^{1/2}(\Gamma)$ such that

$$\begin{aligned}
(\dot{\varphi}_1, \psi_1)_{0,\Omega_1} + \langle \lambda, \psi_1 \rangle_\Gamma + \left(k_1 \tfrac{\partial \varphi_1}{\partial y}, \tfrac{\partial \psi_1}{\partial y}\right)_{0,\Omega_1} + \left(u_1 \tfrac{\partial \varphi_1}{\partial x}, \psi_1\right)_{0,\Omega_1} &= (f_1, \psi_1)_{0,\Omega_1} \quad \forall \psi_1 \in H^1_D(\Omega_1) \\
(\dot{\varphi}_2, \psi_2)_{0,\Omega_2} - \langle \lambda, \psi_2 \rangle_\Gamma + \left(k_2 \tfrac{\partial \varphi_2}{\partial y}, \tfrac{\partial \psi_2}{\partial y}\right)_{0,\Omega_2} + \left(u_2 \tfrac{\partial \varphi_2}{\partial x}, \psi_2\right)_{0,\Omega_2} &= (f_2, \psi_2)_{0,\Omega_2} \quad \forall \psi_2 \in H^1_D(\Omega_2)\,, \\
\langle \alpha(\varphi_1 - \varphi_2) - \lambda, \mu \rangle_\Gamma &= 0 \quad \forall \mu \in H^{-1/2}(\Gamma),
\end{aligned} \tag{2.5}$$

where the function spaces are chosen to enforce the Dirichlet boundary conditions, denoted by the subscript D. The last equation contributes the term $\langle \lambda, \mu \rangle_\Gamma$ which endows (2.5) with the structure of a penalized mixed problem, see, e.g., [25, p. 71] and [21]. This structure relaxes the inf–sup stability requirement of the mixed setting. By treating λ as a separate variable, the system has been lifted to a space with more degrees of freedom. Unlike the standard transmission conditions case which generates a Lagrange multiplier system, in [8], the bulk condition can be substituted back in to the model equations. However, the lifted form of the model equations allows the interface condition to be treated in a special way, separately from the model equations.

3. Partitioned scheme

Discretizing the monolithic mixed problem (2.5) in space we obtain the following semi-discrete problem.

Seek $\{\varphi_1^h, \varphi_2^h, \lambda^h\} \in S^h_{1,D}(\Omega_1) \times S^h_{2,D}(\Omega_2) \times G^h_\Gamma$ such that,

$$\begin{aligned}
\left(\dot{\varphi}_1^h, \psi_1^h\right)_{0,\Omega_1} + \left\langle \lambda^h, \psi_1^h \right\rangle_\Gamma + \left(k_1 \tfrac{\partial \varphi_1^h}{\partial y}, \tfrac{\partial \psi_1^h}{\partial y}\right)_{0,\Omega_1} + \left(u_1 \tfrac{\partial \varphi_1^h}{\partial x}, \psi_1^h\right)_{0,\Omega_1} &= \left(f_1, \psi_1^h\right)_{0,\Omega_1} \quad \forall \psi_1^h \in S^h_{1,D}(\Omega_1) \\
\left(\dot{\varphi}_2^h, \psi_2^h\right)_{0,\Omega_2} - \left\langle \lambda^h, \psi_2^h \right\rangle_\Gamma + \left(k_2 \tfrac{\partial \varphi_2^h}{\partial y}, \tfrac{\partial \psi_2^h}{\partial y}\right)_{0,\Omega_2} + \left(u_2 \tfrac{\partial \varphi_2^h}{\partial x}, \psi_2^h\right)_{0,\Omega_2} &= \left(f_2, \psi_2^h\right)_{0,\Omega_2} \quad \forall \psi_2^h \in S^h_{2,D}(\Omega_2) \\
\left\langle \alpha(\varphi_1^h - \varphi_2^h) - \lambda^h, \mu^h \right\rangle_\Gamma &= 0 \quad \forall \mu^h \in G^h(\Gamma).
\end{aligned} \tag{3.1}$$

Thanks to term $\left\langle \lambda^h, \mu^h \right\rangle_\Gamma$ the flux variable is not subject to an inf–sup stability condition and, compared to a mixed formulation, we have a greater flexibility in the choice of the discrete space G^h_Γ.

The semi-discrete monolithic problem (3.1) is equivalent to the following system of Differential Algebraic Equations (DAEs)

$$\begin{aligned}
M_1 \dot{\boldsymbol{\varphi}}_1 + G_1^T \boldsymbol{\lambda} + K_1 \boldsymbol{\varphi}_1 &= \mathbf{f}_1(t) \\
M_2 \dot{\boldsymbol{\varphi}}_2 - G_2^T \boldsymbol{\lambda} + K_2 \boldsymbol{\varphi}_2 &= \mathbf{f}_2(t) \\
\alpha G_1 \boldsymbol{\varphi}_1 - \alpha G_2 \boldsymbol{\varphi}_2 - \widehat{M}_\Gamma \boldsymbol{\lambda} &= 0\,.
\end{aligned} \tag{3.2}$$

In this setting, $\boldsymbol{\varphi}_1$ and $\boldsymbol{\varphi}_2$ are coefficient vectors of the solutions φ_1^h and φ_2^h and $\boldsymbol{\lambda}$ is the coefficient vector of the flux-variable λ^h. The coefficient matrices for the advection–diffusion operators are denoted by K_i, $i = 1, 2$. Mass matrices for the subdomain spaces are denoted M_i, $i = 1, 2$, the interface mass matrix is designated $\widehat{M}_\Gamma$, and G_i, $i = 1, 2$ are rectangular matrices with elements given by

$$(G_i)_{qr} = \langle \psi^h_{i,q}, \mu^h_r \rangle_\Gamma, \quad q = 1, \ldots, n_i, \quad r = 1, \ldots, |G^h|; \quad i = 1, 2.$$

If instead of the bulk coupling condition (2.4) our monolithic problem were to employ a perfect interface condition the last equation in (3.2) would read

$$G_1 \boldsymbol{\varphi}_1 - G_2 \boldsymbol{\varphi}_2 = 0\,, \tag{3.3}$$

and the monolithic problem would be a Hessenberg Index-2 DAE. In this case, one can differentiate (3.3) to obtain an alternate constraint on the time derivative of the solution:

$$G_1 \dot{\boldsymbol{\varphi}}_1 - G_2 \dot{\boldsymbol{\varphi}}_2 = 0\,. \tag{3.4}$$

Substitution of (3.3) with (3.4) transforms the monolithic problem into a Hessenberg Index-1 DAE. This makes it possible to solve for the algebraic variable $\boldsymbol{\lambda}$ in terms of the states $\boldsymbol{\varphi}_1$ and $\boldsymbol{\varphi}_2$. Application of an explicit time integration scheme to the monolithic problem then effectively decouples it into two independent equations, one for each subdomain. This approach was followed in [8] to develop the IVR coupling approach.

In the case with the bulk interface coupling condition (2.4), the additional term ($\widehat{M}_\Gamma \boldsymbol{\lambda}$) that helps assuage the stability restrictions of the mixed setting also prevents us from applying the IVR time differentiation "trick" directly to the semidiscrete problem (3.2). Instead, we will first discretize (3.2) in time to generate a fully discrete monolithic formulation from which we can obtain $\boldsymbol{\lambda}$ by constructing a Schur complement similar to the one in the IVR approach. Furthermore, unlike IVR where explicit time stepping was required to decouple the equations, we now have the flexibility to "mix-and-match" explicit and/or implicit time discretizations in each domain. This flexibility is inherited from the fact that the bulk

condition case is a lifted PDE and not a Lagrange multiplier system. Specifically, we allow for the possibility of an explicit method in one domain and an implicit method in the other. If the same time-stepping method is used in both domains, the time discretization for the bulk condition is clear by substituting it back into the model equations. However, if the time-stepping methods in each domain are different, the discretization for the bulk condition is not clear. For this reason, we allow the bulk condition to be discretized in time separately from the model equations in the Bulk-IFR method. In some cases, this can be thought of as a semi-implicit method, where the coupling conditions receive special treatment. This is especially useful when mixing explicit and implicit time-stepping methods, where treating the bulk condition explicitly could lead to instabilities. In this situation, one does not expect optimal accuracy because the coupling term is treated implicitly in the explicit method. Discovering discretizations for the bulk condition that are both stable and optimally accurate are a topic of future research. Another option is to use an implicit discretization in one domain for the bulk condition and an explicit discretization in the other, with respect to the each domains' time-discretization [17]. While this treatment is stable and efficient, in general, the method does not conserve flux. To achieve conservation on matching grids, the Bulk-IFR method uses a single flux, λ, for both domains.

To demonstrate the flexibility of the Bulk-IFR method in the choice of implicit and explicit methods, we discretize the equations using the θ–method, with a different $\theta_i \in [0, 1]$ for each domain. This general approach gives rise to a family of time-discretizations. We could choose to discretize the bulk condition with the θ–method as well, but for the sake of flexibility we choose a backward Euler discretization. In fact, if both domains' models are discretized with backward Euler, this choice of discretization for the bulk condition leads a consistent monolithic backward Euler method. Moreover, the Bulk-IFR method does this while still decoupling the domains' model equations. Of course, a more general formulation could be given that encompasses multi-stage and multi-step methods. However, the θ–method suffices to demonstrate how the Bulk-IFR method handles heterogeneous time-integration across the interface in a simple manner, and the procedure generalizes for any single stage method. For multi-stage methods, the decoupling strategy is not as clear. One must either perform the Bulk-IFR method at all or some of the stages, with the remaining stages treat the bulk condition with the native multi-stage approximation. In the worse case-scenario, the decoupling strategy is not as effective. Constructing approximations of the flux which are well suited for multi-stage methods are reserved for future research.

The θ–method discretization of the system in (3.2) gives the following fully discrete monolithic formulation:

$$\begin{aligned} M_1\left(\boldsymbol{\varphi}_1^{n+1}-\boldsymbol{\varphi}_1^{n}\right)/\Delta t + K_1\left(\theta_1\boldsymbol{\varphi}_1^{n+1}+(1-\theta_1)\boldsymbol{\varphi}_1^{n}\right) + G_1^T\boldsymbol{\lambda}^{n+1} &= \theta_1\mathbf{f}_1(t^{n+1})+(1-\theta_1)\mathbf{f}_1(t^n)\,, \\ M_2\left(\boldsymbol{\varphi}_2^{n+1}-\boldsymbol{\varphi}_2^{n}\right)/\Delta t + K_2\left(\theta_2\boldsymbol{\varphi}_2^{n+1}+(1-\theta_2)\boldsymbol{\varphi}_2^{n}\right) - G_2^T\boldsymbol{\lambda}^{n+1} &= \theta_2\mathbf{f}_2(t^{n+1})+(1-\theta_2)\mathbf{f}_2(t^n) \\ \alpha G_1\boldsymbol{\varphi}_1^{n+1} - \alpha G_2\boldsymbol{\varphi}_2^{n+1} - \widehat{M}_\Gamma\boldsymbol{\lambda}^{n+1} &= 0\,. \end{aligned} \tag{3.5}$$

If we define the following matrix

$$W_i = M_i + \Delta t\theta_i K_i\,,$$

and reform the right hand sides as

$$\mathbf{g}_i(\boldsymbol{\varphi}_i^n) = \Delta t(\theta_i\mathbf{f}_i(t^{n+1})+(1-\theta_i)(\mathbf{f}_i(t^n)-K\boldsymbol{\varphi}_i^n))+M_i\boldsymbol{\varphi}_i^n\,,$$

then the monolithic problem (3.5) is equivalent to the following linear system of equations

$$\begin{bmatrix} W_1 & 0 & \Delta t G_1^T \\ 0 & W_2 & -\Delta t G_2^T \\ \alpha G_1 & -\alpha G_2 & -\widehat{M}_\Gamma \end{bmatrix} \begin{bmatrix} \boldsymbol{\varphi}_1^{n+1} \\ \boldsymbol{\varphi}_2^{n+1} \\ \boldsymbol{\lambda} \end{bmatrix} = \begin{bmatrix} \mathbf{g}_1(\boldsymbol{\varphi}_1^n) \\ \mathbf{g}_2(\boldsymbol{\varphi}_2^n) \\ 0 \end{bmatrix}. \tag{3.6}$$

In the next section we present the decoupling of (3.6) in the general case and then consider the case when both subdomain equations are discretized by an explicit time integrator. The case where an explicit time integrator is used in one domain and implicit in the other be easily inferred from these examples, and for this reason is omitted.

3.1. The general case

We first reorder (3.6) by grouping together the solution coefficients in the interior of the domain, designated by subscript 0, and the coefficients on the interface, designated by subscript Γ. The remaining undefined subscripts, $\Gamma 0$ and 0Γ identify the parts of the mass matrix from the interior to the boundary and vice-versa, respectively. The reordered monolithic system then assumes the following form:

$$\begin{bmatrix} W_{1,\Gamma} & 0 & \Delta t G_1^T & W_{1,\Gamma 0} & 0 \\ 0 & W_{2,\Gamma} & -\Delta t G_2^T & 0 & W_{2,\Gamma 0} \\ \alpha G_1 & -\alpha G_2 & \widehat{M}_\Gamma & 0 & 0 \\ W_{1,0\Gamma} & 0 & 0 & W_{1,0} & 0 \\ 0 & W_{2,0\Gamma} & 0 & 0 & W_{2,0} \end{bmatrix} \begin{bmatrix} \boldsymbol{\varphi}_{1,\Gamma}^{n+1} \\ \boldsymbol{\varphi}_{2,\Gamma}^{n+1} \\ \boldsymbol{\lambda} \\ \boldsymbol{\varphi}_{1,0}^{n+1} \\ \boldsymbol{\varphi}_{2,0}^{n+1} \end{bmatrix} = \begin{bmatrix} \mathbf{g}_{1,\Gamma}(\boldsymbol{\varphi}_1^n) \\ \mathbf{g}_{2,\Gamma}(\boldsymbol{\varphi}_2^n) \\ 0 \\ \mathbf{g}_{1,0}(\boldsymbol{\varphi}_1^n) \\ \mathbf{g}_{2,0}(\boldsymbol{\varphi}_2^n) \end{bmatrix}. \tag{3.7}$$

Note that we abuse the notation slightly by using G_i in both the full system and interface-partitioned system. In fact, the G_i operators in (3.7) are now absent of non-interface degrees of freedom, which are simply zero in the larger representation of G_i. Performing a Schur complement, we have the following reduced linear system for degrees of freedom on the interface

$$\begin{bmatrix} A_{1,\Gamma} & 0 & \Delta t G_1^T \\ 0 & A_{2,\Gamma} & -\Delta t G_2^T \\ \alpha G_1 & -\alpha G_2 & -\widehat{M}_\Gamma \end{bmatrix} \begin{bmatrix} \boldsymbol{\varphi}_{1,\Gamma}^{n+1} \\ \boldsymbol{\varphi}_{2,\Gamma}^{n+1} \\ \boldsymbol{\lambda} \end{bmatrix} = \begin{bmatrix} \widehat{\mathbf{g}}_{1,\Gamma}(\boldsymbol{\varphi}_1^n) \\ \widehat{\mathbf{g}}_{2,\Gamma}(\boldsymbol{\varphi}_2^n) \\ 0 \end{bmatrix}, \tag{3.8}$$

where A_i and $\widehat{\mathbf{g}}_{i,\Gamma}$ are generalized mass matrices and force vectors given by

$$A_{1,\Gamma} = W_{1,\Gamma} - W_{1,\Gamma 0} W_{1,0}^{-1} W_{1,0\Gamma} \quad \text{and} \quad A_{2,\Gamma} = W_{2,\Gamma} - W_{2,\Gamma 0} W_{2,0}^{-1} W_{2,0\Gamma},$$

$$\widehat{\mathbf{g}}_{1,\Gamma}(\boldsymbol{\varphi}_1^n) = \mathbf{g}_{1,\Gamma}(\boldsymbol{\varphi}_1^n) - W_{1,\Gamma 0} W_{1,0}^{-1} \mathbf{g}_{1,0}(\boldsymbol{\varphi}_1^n) \quad \text{and} \quad \widehat{\mathbf{g}}_{2,\Gamma}(\boldsymbol{\varphi}_2^n) = \mathbf{g}_{2,\Gamma}(\boldsymbol{\varphi}_2^n) - W_{2,\Gamma 0} W_{2,0}^{-1} \mathbf{g}_{2,0}(\boldsymbol{\varphi}_2^n),$$

We can then solve for $\boldsymbol{\lambda}$ as

$$\begin{aligned} \boldsymbol{\lambda} &= \left(\alpha \Delta t G_1^T A_{1,\Gamma}^{-1} G_1 + \alpha \Delta t G_2^T A_{2,\Gamma}^{-1} G_2 - \widehat{M}_\Gamma\right)^{-1} \left(\alpha \Delta t G_1^T A_{1,\Gamma}^{-1} \widehat{\mathbf{g}}_{1,\Gamma}(\boldsymbol{\varphi}_1^n) - \alpha \Delta t G_2^T A_{2,\Gamma}^{-1} \widehat{\mathbf{g}}_{2,\Gamma}(\boldsymbol{\varphi}_2^n)\right) \\ &= S^{-1} \left(\alpha \Delta t G_1^T A_{1,\Gamma}^{-1} \widehat{\mathbf{g}}_{1,\Gamma}(\boldsymbol{\varphi}_1^n) - \alpha \Delta t G_2^T A_{2,\Gamma}^{-1} \widehat{\mathbf{g}}_{2,\Gamma}(\boldsymbol{\varphi}_2^n)\right), \end{aligned} \tag{3.9}$$

where S is the Schur complement matrix. Now the flux $\boldsymbol{\lambda}^{n+1}$ can be inserted into the full monolithic system and $\boldsymbol{\varphi}_1^{n+1}$ and $\boldsymbol{\varphi}_2^{n+1}$ can be found independently in a decoupled fashion, while treating $\boldsymbol{\lambda}^{n+1}$ as boundary condition on Γ.

3.2. The explicit case

Choosing the time integrator to be explicit in each domain, i.e., setting $\theta_1 = 0$ and $\theta_2 = 0$, reduces the linear system in (3.6) to

$$\begin{bmatrix} M_1 & 0 & \Delta t G_1^T \\ 0 & M_2 & -\Delta t G_2^T \\ \alpha G_1 & -\alpha G_2 & -\widehat{M}_\Gamma \end{bmatrix} \begin{bmatrix} \boldsymbol{\varphi}_1^{n+1} \\ \boldsymbol{\varphi}_2^{n+1} \\ \boldsymbol{\lambda} \end{bmatrix} = \begin{bmatrix} \mathbf{g}_1(\boldsymbol{\varphi}_1^n) \\ \mathbf{g}_2(\boldsymbol{\varphi}_2^n) \\ 0 \end{bmatrix}. \tag{3.10}$$

After reordering (3.10) to separate out the components in the interior of the domain, indexed by 0, and the components on the interface, indexed by Γ we arrive at the following linear system

$$\begin{bmatrix} M_{1,\Gamma} & 0 & \Delta t G_1^T & M_{1,\Gamma 0} & 0 \\ 0 & M_{2,\Gamma} & -\Delta t G_2^T & 0 & M_{2,\Gamma 0} \\ \alpha G_1 & -\alpha G_2 & \widehat{M}_\Gamma & 0 & 0 \\ M_{1,0\Gamma} & 0 & 0 & M_{1,0} & 0 \\ 0 & M_{2,0\Gamma} & 0 & 0 & M_{2,0} \end{bmatrix} \begin{bmatrix} \boldsymbol{\varphi}_{1,\Gamma}^{n+1} \\ \boldsymbol{\varphi}_{2,\Gamma}^{n+1} \\ \boldsymbol{\lambda} \\ \boldsymbol{\varphi}_{1,0}^{n+1} \\ \boldsymbol{\varphi}_{2,0}^{n+1} \end{bmatrix} = \begin{bmatrix} \mathbf{g}_{1,\Gamma}(\boldsymbol{\varphi}_1^n) \\ \mathbf{g}_{2,\Gamma}(\boldsymbol{\varphi}_2^n) \\ 0 \\ \mathbf{g}_{1,0}(\boldsymbol{\varphi}_1^n) \\ \mathbf{g}_{2,0}(\boldsymbol{\varphi}_2^n) \end{bmatrix}. \tag{3.11}$$

In the case of a lumped mass matrix, $M_{1,\Gamma 0}$, $M_{2,\Gamma 0}$, $M_{1,0\Gamma}$, and $M_{2,0\Gamma}$ are identically zero and we have the reduced linear system over the interface

$$\begin{bmatrix} M_{1,\Gamma} & 0 & \Delta t G_1^T \\ 0 & M_{2,\Gamma} & -\Delta t G_2^T \\ \alpha G_1 & -\alpha G_2 & -\widehat{M}_\Gamma \end{bmatrix} \begin{bmatrix} \boldsymbol{\varphi}_{1,\Gamma}^{n+1} \\ \boldsymbol{\varphi}_{2,\Gamma}^{n+1} \\ \boldsymbol{\lambda} \end{bmatrix} = \begin{bmatrix} \mathbf{g}_{1,\Gamma}(\boldsymbol{\varphi}_1^n) \\ \mathbf{g}_{2,\Gamma}(\boldsymbol{\varphi}_2^n) \\ 0 \end{bmatrix}. \tag{3.12}$$

We can then solve for $\boldsymbol{\lambda}$ as

$$\boldsymbol{\lambda} = \left(\alpha \Delta t G_1^T M_{1,\Gamma}^{-1} G_1 + \alpha \Delta t G_2^T M_{2,\Gamma}^{-1} G_2 - \widehat{M}_\Gamma\right)^{-1} \left(\alpha \Delta t G_1^T M_{1,\Gamma}^{-1} \mathbf{g}_{1,\Gamma}(\boldsymbol{\varphi}_1^n) - \alpha \Delta t G_2^T M_{2\Gamma}^{-1} \mathbf{g}_{2,\Gamma}(\boldsymbol{\varphi}_2^n)\right). \tag{3.13}$$

Note that in this case, the Schur complement is almost trivial to construct because it only involves inverses of diagonal matrices.

In the case of a consistent mass matrix, we have the following reduced linear system

$$\begin{bmatrix} \bar{A}_{1,\Gamma} & 0 & \Delta t G_1^T \\ 0 & \bar{A}_{2,\Gamma} & -\Delta t G_2^T \\ \alpha G_1 & -\alpha G_2 & -\widehat{M}_\Gamma \end{bmatrix} \begin{bmatrix} \boldsymbol{\varphi}_{1,\Gamma}^{n+1} \\ \boldsymbol{\varphi}_{2,\Gamma}^{n+1} \\ \boldsymbol{\lambda} \end{bmatrix} = \begin{bmatrix} \widehat{\mathbf{g}}_{1,\Gamma}(\boldsymbol{\varphi}_1^n) \\ \widehat{\mathbf{g}}_{2,\Gamma}(\boldsymbol{\varphi}_2^n) \\ 0 \end{bmatrix}. \tag{3.14}$$

where $A_{i,\Gamma}$ and $\widehat{\mathbf{g}}_{i,\Gamma}$ are generalized mass matrices and force vectors given by

$$\bar{A}_{1,\Gamma} = M_{1,\Gamma} - M_{1,\Gamma 0} M_{1,0}^{-1} M_{1,0\Gamma} \quad \text{and} \quad \bar{A}_{1,\Gamma} = M_{2,\Gamma} - M_{2,\Gamma 0} M_{2,0}^{-1} M_{2,0\Gamma};$$

$$\widehat{\mathbf{g}}_{1,\Gamma}(\boldsymbol{\varphi}_1) = \mathbf{g}_{1,\Gamma}(\boldsymbol{\varphi}_1) - M_{1,\Gamma 0} M_{1,0}^{-1} \mathbf{g}_{1,0}(\boldsymbol{\varphi}_1) \quad \text{and} \quad \widehat{\mathbf{g}}_{2,\Gamma}(\boldsymbol{\varphi}_2) = \mathbf{g}_{2,\Gamma}(\boldsymbol{\varphi}_2) - M_{2,\Gamma 0} M_{2,0}^{-1} \mathbf{g}_{2,0}(\boldsymbol{\varphi}_2),$$

From this linear system an equation for $\boldsymbol{\lambda}$ analogous to Eq. (3.13) is obtained. Because we consider advection, we will not consider mass lumping.

4. Simplified ocean-atmosphere test case

Motivated by the test case forcing in [19] (Q in Section 4), we present a test case which represents the heat exchange between the ocean and atmosphere. The model used is the advection–diffusion equation for the temperature and a prescribed velocity, as described in Section 2.

4.1. Domain

We choose the spatial domain to be a rectangular domain such that $(x, y) \in [0, x_{\max}] \times [-y_{\max}, y_{\max}]$. To model the ocean–atmosphere interface, the domain will lie approximately on the mixing layers of the atmosphere and ocean and span a large distance in the x direction. The parameters defining the domain are $x_{\max} = 10$ km and $y_{\max} = 500$ m. The atmospheric domain is given by $\Omega_1 = [0, x_{\max}] \times [0, y_{\max}]$ and the oceanic domain is given by $\Omega_2 = [0, x_{\max}] \times [-y_{\max}, 0]$. This choice leads to the interface Γ lying on the line $y(x) = 0$.

4.2. Analytic solution

Following [19], we set the forcing in the atmosphere to be a sinusoid and the forcing in the ocean to be zero. Physically speaking, this choice in the forcing is such that it models radiative heating and heat dissipation in the atmosphere, and no radiative heating in the ocean. Certain properties are desired in the solution for physical reasons:

1. $\varphi_i > 0$ because the solution is a temperature.
2. The bulk condition is to be satisfied non-trivially, i.e., the solution must have a jump at Γ.
3. The solution must be some small variation about some constant temperature which is comparable to variations seen in the ocean–atmosphere system.

Let us choose a general sinusoidal form for the forcing in the atmosphere f_1, e.g.,

$$f_1(x, t) = A \cos\left(N\pi(x - u_1 t)\right),$$

where $N \in \mathbb{Q}$. To find the solution of (2.1), we construct an advection equation and a Poisson equation in order to make a reasonable ansatz about the solution of (2.1). This is a suitable strategy since the advection and diffusion operators act in mutually orthogonal directions. We will also assume that diffusivities k_i are constants. This gives

$$\frac{\partial \tilde{\varphi}_1}{\partial t} + u_1 \frac{\partial \tilde{\varphi}_1}{\partial x} = 0 \tag{4.1}$$

$$-k_1 \frac{\partial^2 \hat{\varphi}_1}{\partial y^2} = f_1 , \tag{4.2}$$

Clearly, choosing

$$\tilde{\varphi}_1(x, t) = \frac{1}{N\pi} f_1 + c_1 ,$$

satisfies the advection equation, and choosing

$$\hat{\varphi}(y) = -\frac{1}{2k_1}(y - a)^2 f_1 + c_2 y + c_3 ,$$

satisfies the Poisson equation, where a, c_1, c_2, and c_3 are constants. Neglecting the linear term in $\hat{\varphi}$, a reasonable ansatz for φ_1 is

$$\varphi_1 = -\frac{A'}{2N\pi k_1} \cos(N\pi(x - u_1 t))(y - a)^2 + T_1,$$

where $c_3 = T_1$ is chosen such that $\varphi_1 > 0$ and gives a temperature profile seen in the atmosphere near the ocean. This ansatz constrains A to be

$$A = \frac{A'}{N\pi} .$$

To find φ_2, the previous approach is repeated for $f_2 = 0$. For the given forcing, the Poisson equation reduces to a Laplace equation. We choose our ansatz for φ_2 to have a linear dependence on y. A reasonable ansatz for φ_2 is then given by

$$\varphi_2 = \frac{B'}{N\pi k_2} \cos(N\pi(x - u_2 t))(y - b) + T_2 ,$$

where b and T_2 are constants. Our ansatz on the φ_1 and φ_2 satisfy the model equations, but they also need to satisfy the bulk condition, given in (2.4). The bulk condition asserts that

$$\begin{aligned} -\frac{A'}{N\pi}\cos(N\pi(x-u_1t))(y-a) &= \frac{B'}{N\pi}\cos(N\pi(x-u_2t)) \\ = \alpha(-\frac{A'}{2N\pi k_1}\cos(N\pi(x-u_1t))(y-a)^2 &- \frac{B'}{N\pi k_2}\cos(N\pi(x-u_2t))(y+b)+(T_1-T_2)) \quad \text{on } \Gamma\,. \end{aligned}$$

Recall that Γ is given by the line $y(x)=0$. Inserting this into the bulk condition gives

$$\begin{aligned} \frac{A'}{N\pi}\cos(N\pi(x-u_1t))a &= \frac{B'}{N\pi}\cos(N\pi(x-u_2t)) \\ &= \alpha\left(-\frac{A'}{2N\pi k_1}\cos(N\pi(x-u_1t))a^2 - \frac{B'}{N\pi k_2}\cos(N\pi(x-u_2t))b+(T_1-T_2)\right)\,, \end{aligned}$$

which can be satisfied if $u_1=u_2=u$

$$\begin{aligned} \frac{aA'}{N\pi}\cos(N\pi(x-ut)) &= \frac{B'}{N\pi}\cos(N\pi(x-ut)) \\ &= \alpha\left(-a^2\frac{A'}{2N\pi k_1}\cos(N\pi(x-ut)) - \frac{B'}{N\pi k_2}\cos(N\pi(x-ut))b+(T_1-T_2)\right)\,. \end{aligned}$$

This simplifies to

$$\frac{aA'}{N\pi} = \frac{B'}{N\pi} = \alpha\left(-a^2\frac{A'}{2N\pi k_1} - \frac{B'}{N\pi k_2}b + (T_1-T_2)\sec(N\pi(x-ut))\right).$$

The relation above will lead to α having space and time dependence. We make α constant by letting $T_1=T_2=T$. This gives

$$\frac{aA'}{N\pi} = \frac{B'}{N\pi} = \alpha\left(-a^2\frac{A'}{2N\pi k_1} - \frac{B'}{N\pi k_2}b\right).$$

from where one can easily determine the relations

$$B' = A'a\,,$$

and

$$\alpha = -\frac{A'a}{\left(\frac{a^2A'}{2k_1}+\frac{B'}{k_2}b\right)},$$

respectively. Although the parameter α is a constant and does not contain the jump in the velocities of the two models, as is the case for the physical bulk condition [17], this test case is still suitable to test the Bulk-IFR method on a Robin boundary condition. In fact, choosing α to contain the jump in the velocities will not change the structure of problem, but makes finding an analytical solution more difficult.

4.3. Physical parameters

We now specify values for the parameters based on physical assumptions, which are summarized in Table 1. We choose the constant T to be 293.15 K. The thermal diffusivities for air and seawater can be found readily in the literature and are temperature dependent. However, for turbulent flows, the diffusivities can be much higher than those in laminar flows. For the manufactured solution, the thermal diffusivities only scale the solution and change the CFL. So using an arbitrary value instead an exact value from ocean–atmosphere system only changes the scaling of the solution. The values of the diffusivities and the size of the discontinuity at the interface determine the magnitude of the flux across the interface, and hence define the strength of the coupling. For this reason, we will vary the value of the diffusivities in the numerical tests, to evaluate the Bulk-IFR method at different coupling strengths. One should note that the physical values specified in [17] are in the range of values that we choose. Moreover, we do not choose extremely small diffusivities as this would lead to an extremely small flux across the interface and decouple the sub-problems.

4.4. Free parameters

As of now the parameters a, b, A' and N have not yet been defined. These parameters will be constrained so that the solution is realistic and meets the criteria set in 4.2. The value of N controls the frequency of the forcing and therefore the solution. We arbitrarily choose $N=\frac{1}{1000}$ so that the wave has a period of 5 over the domain at $t=0$. We choose $b=-y_{\max}$ so that amplitude of φ_2 is largest at the surface and goes to the constant value of T as the bottom of the domain is reached. This is done to model the more chaotic upper ocean and the more steady temperatures at deeper depths.

Table 1
Model parameters for the simplified ocean–atmosphere test-case.

Parameter	Value
T	293.15 K = 20 °C
u	1 m s^{-1}
M_1	2 K
M_2	0.5 K

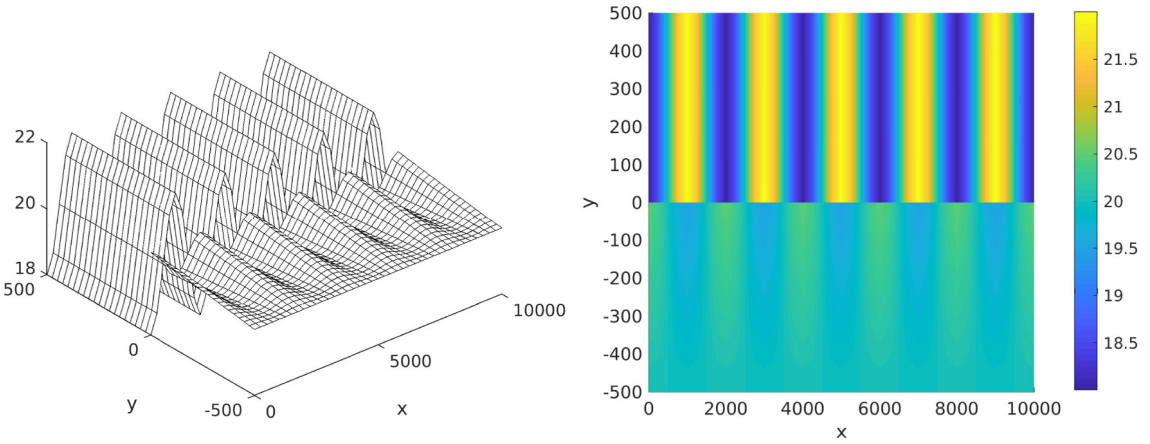

Fig. 2. Surface and density plot of the solution (φ_1, φ_2), (top, bottom), at $t = 0$. The domain is given in meters and the solution in given in degrees Celsius.

Finally, we desire that the solution is a small variation around some constant value. The parameters B' and A' are coupled by the bulk condition, thus there are two free parameters left, a and B', that allow us to control the variation in temperature. The value B' can be chosen in such a way that this property is ensured. The maximum amplitude of ϕ_2 about T occurs at $y = 0$ and is given by

$$\max |\varphi_2 - T| = \left(\frac{B' y_{\max}}{N\pi k_2}\right) = M_2 \, .$$

A maximum amplitude of M_2 in φ_2, about T, is achieved by choosing B' to be

$$B' = \frac{M_2 N\pi k_2}{y_{\max}}.$$

The maximum amplitude of φ_1 about T is given by

$$\max |\varphi_1 - T| = \frac{A' a^2}{2N\pi k_1} = M_1 \, . \tag{4.3}$$

From the bulk condition, the value of A' is constrained to be

$$A' = \frac{B'}{a} \, .$$

Substituting this into (4.3) gives

$$\frac{B' a}{2N\pi k_1} = M_1 \, .$$

Thus to achieve a maximum amplitude of M_1 in φ_1, about T, a is constrained to be

$$a = \frac{2M_1 N\pi k_1}{B'} \, .$$

Now that all the parameters have been specified, except the diffusivities, we can visualize the initial condition of the solution. A surface and density plot of φ_1 (top) and φ_2 (bottom) are show in Fig. 2.

5. Numerical results

The test case in the previous section is implemented using the finite element method in space and the forward Euler method in time. For simplicity Lagrange, piece-wise linear elements on rectangles were chosen. The space G^h_Γ for the

Table 2
The grid size in the x and y direction, the time-step, the relative error in the L^2 norm, the relative error in the H^1 semi-norm, and the convergence rates between the two finest meshes for $k_1 = 0.1$ and $k_2 = 2$.

$k_1 = 0.1$ m^2 s^{-1}	$k_2 = 2$ m^2 s^{-1}	α = 4e−4 m s^{-1}		
h_x	h_y	Δt	L_2	H_1 SN
333	33.3	1.06	5.059e−03	2.967e−01
166	16.6	0.52	1.216e−03	1.488e−01
83.3	8.33	0.26	2.923e−04	7.458e−02
Rate	–	–	2.057	0.997

Table 3
The grid size in the x and y direction, the time-step, the relative error in the L^2 norm, the relative error in the H^1 semi-norm, and the convergence rates between the two finest meshes for $k_1 = 1$ and $k_2 = 20$.

$k_1 = 1$ m^2 s^{-1}	$k_2 = 20$ m^2 s^{-1}	α = 4e−3 m s^{-1}		
h_x	h_y	Δt	L_2	H_1 SN
333	33.3	1.06	5.000e−03	2.953e−01
166	16.6	0.53	1.198e−03	1.488e−01
83.3	8.33	0.17	2.906e−04	7.262e−02
Rate	–	–	2.043	1.034

Table 4
The grid size in the x and y direction, the time-step, the relative error in the L^2 norm, the relative error in the H^1 semi-norm, and the convergence rates between the two finest meshes for $k_1 = 10$ and $k_2 = 200$.

$k_1 = 10$ m^2 s^{-1}	$k_2 = 200$ m^2 s^{-1}	α = 4e−2 m s^{-1}		
h_x	h_y	Δt	L_2	H_1 SN
333	33.3	0.277	4.718e−03	2.993e−01
166	16.6	0.069	1.261e−03	1.547e−01
83.3	8.33	0.017	4.124e−04	8.085e−02
Rate	–	–	2.057	0.997

auxiliary variable $\boldsymbol{\lambda}$ on the interface must also be specified. It can chosen to be the trace space, on Γ, of either S_1^h, $\Gamma(\Omega_1)$ or S_2^h, $\Gamma(\Omega_2)$, or the union of their trace spaces. However, stability is not guaranteed if the union of the spaces is chosen. For this reason, if the meshes on the two domains are not the same, the trace space on one side of the interface will be chosen. We also use the SUPG method to ensure stability, because of the consideration of advective processes. We follow the same procedure for SUPG as in [8].

5.1. Convergence study in space

The first test we consider is the convergence in space of the Bulk-IFR method with different strengths of diffusion. The time horizon was chosen to be 100 s, and the time-step was chosen to be $\Delta t = 0.01\Delta t_{\text{CFL}}$, where Δt_{CFL} corresponds to a Courant number of one for the most restrictive CFL condition between the advection and diffusion terms. Thus the time-step is refined with respect to the CFL condition so that the time-discretization error does not pollute the spatial-discretization convergence.

The convergence results are given in Table 2 for $k_1 = 0.1$ and $k_2 = 2$, Table 3 for $k_1 = 1$ and $k_2 = 20$, Table 4 for $k_1 = 10$ and $k_2 = 200$, and Table 5 for $k_1 = 1\text{e}4$ and $k_2 = 2\text{e}4$. Each table also provides the corresponding value of α. The value of α and the magnitude of the discontinuity, given by M_1 and M_2 decide the magnitude of the flux. The relative errors are given in the L^2 and H^1 semi-norm. To show the convergence, the semi-norm is given as opposed to the H^1 norm because the error in semi-norm is much smaller than in the L^2, in an absolute sense. In all cases we observe that the Bulk-IFR coupler maintains optimal theoretic rates of convergence for the bilinear finite elements employed in the test.

5.2. Non-matching resolution in grids

In general, the climate model's component's models use different grids whose resolutions are adapted to the physics of each component. Thus, in order for the Bulk-IFR scheme to be useful for ocean–atmosphere coupling it must be able to handle different grid resolutions. To verify this, the next test considers spatial convergence when the two subdomains' grids have different resolutions.

The time horizon was chosen to be 100 s, and the time-step was chosen to be $\Delta t = 0.01\Delta t_{\text{CFL}}$, where Δt_{CFL} corresponds to a Courant number of one for the most restrictive CFL condition between the advection and diffusion terms. Thus, the time-step is refined with respect to the CFL condition so that the time-discretization error does not interfere with the

Table 5
The grid size in the x and y direction, the time-step, the relative error in the L^2 norm, the relative error in the H^1 semi-norm, and the convergence rates between the two finest meshes for $k_1 = 1e4$ and $k_2 = 2e4$.

$k_1 = 1e4$ m^2 s^{-1}	$k_2 = 2e4$ m^2 s^{-1}	$\alpha = 4$ m s^{-1}		
h_x	h_y	Δt	L_2	H_1 SN
333	33.3	2.77e−3	4.233e−03	2.931e−01
166	16.6	6.94e−4	1.075e−03	1.4811e−01
83.3	8.33	1.76e−4	2.691e−04	7.4263e−02
Rate	–	–	2.057	0.997

Table 6
The grid size in the x and y direction for Ω_1 and Ω_2, the time-step, the relative error in the L^2 norm, the relative error in H^1 semi-norm, and the convergence rates between the two finest meshes $k_1 = 1$ and $k_2 = 20$. The degrees of freedom for Ω_1 on the interface are used for the auxiliary equation.

$k_1 = 1$ m^2 s^{-1}	$k_2 = 20$ m^2 s^{-1}	$\alpha = 4e{-}3$ m s^{-1}				
$h_{x,1}$	$h_{y,1}$	$h_{x,2}$	$h_{y,2}$	Δt	L_2	H_1 SN
66.6	6.66	333	33.3	0.11	7.516e−04	7.431e−02
33.2	3.32	166	16.6	0.02	1.821e−04	3.697e−02
Rate	–	–	–	–	2.045	1.007

Table 7
The grid size in the x and y direction for Ω_1 and Ω_2, the time-step, the relative error in the L^2 norm, the relative error in H^1 semi-norm, and the convergence rates between the two finest meshes $k_1 = 1$ and $k_2 = 20$. The degrees of freedom for Ω_2 on the interface are used for the auxiliary equation.

$k_1 = 1$ m^2 s^{-1}	$k_2 = 20$ m^2 s^{-1}	$\alpha = 4e{-}3$ m s^{-1}				
$h_{x,1}$	$h_{y,1}$	$h_{x,2}$	$h_{y,2}$	Δt	L_2	H_1 SN
66.6	6.66	333	33.3	0.11	7.522e−04	7.443e−02
33.2	3.32	166	16.6	0.02	1.836e−04	3.790e−02
Rate	–	–	–	–	2.034	0.973

spatial-discretization convergence. For this test, Ω_1 is chosen to be five times finer than Ω_2 so that the set of degrees of freedom on one side of the interface are not a super-set of the other side.

We perform the convergence tests with two different choices of discretizations for the flux variable in the interface equation, corresponding to the traces of the finite element spaces from each subdomain. In the first test we use the trace of the space defined on the finer mesh on Ω_1 and in the second test we discretize the flux using the trace of the space on the coarser mesh in Ω_2. The convergence results for these tests are shown in Tables 6 and 7, respectively. In both cases the convergence rates match the expected theoretical rates of the bilinear elements used for the tests.

6. Conclusions

In this work, we have extended the IVR method in [8] to the bulk coupling condition in ocean–atmosphere dynamics. The extension differs from the IVR method in a non-trivial way. For this reason, we refer to this method as the Bulk-IFR method. The Bulk-IFR method is applicable to both explicit and implicit time-stepping methods through the use of the $\theta-$method time discretization. However, for simplicity, we only demonstrated the Bulk-IFR method with explicit time-stepping schemes in the numerical results. We applied the Bulk-IFR coupler to a coupled system comprising two advection–diffusion equations with advection in the horizontal direction and diffusion in the vertical direction. This problem configuration can be viewed as a simple heat transfer model in the ocean–atmosphere interface which is driven by the bulk condition.

The Bulk-IFR method was demonstrated on a simplified test case with an exact solution for the bulk condition. The test case consists of a wave in the horizontal direction with a discontinuity across the interface. The discontinuity drives the flux across the interface in the bulk condition. Convergences tests were performed using the Bulk-IFR method for different magnitudes of diffusion, which lead to different magnitudes in flux across the interface. The Bulk-IFR method was also evaluated on non-matching grids for the two subdomains. In all cases, the expected convergence rates were achieved.

Although we have demonstrated the Bulk-IFR method for a simplified ocean–atmosphere model of heat transfer, there is still much research to be done. In particular, applying the Bulk-IFR method with implicit or semi-implicit methods is of great interest. Typically the diffusion in these types of models is treated implicitly to avoid the restrictive CFL condition associated with the diffusion. Therefore, the Bulk-IFR method's performance under these conditions is critical for any success for the method in real world applications. Another challenge for the method is the application to the bulk condition existing in the velocity equations in the ocean–atmosphere system. The bulk condition is non-linear in this case, and thus the Bulk-IFR method would require modification to be efficient. All these topics will be critical points in future research.

CRediT authorship contribution statement

K. Chad Sockwell: Conceptualization, Methodology, Software, Writing. **Kara Peterson:** Conceptualization, Methodology, Software, Writing. **Paul Kuberry:** Conceptualization, Methodology, Software, Writing. **Pavel Bochev:** Conceptualization, Methodology, Software, Supervision, Writing. **Nat Trask:** Conceptualization, Methodology, Software.

Declaration of competing interest

The authors declare that they have no known competing financial interests or personal relationships that could have appeared to influence the work reported in this paper.

Acknowledgments

This material is based upon work supported by the U.S. Department of Energy, Office of Science, Office of Advanced Scientific Computing Research; United States under Award Number DE-SC-0000230927, and the Coupling Approaches for Next-Generation Architectures (CANGA) project, a joint effort funded by the United States Department of Energy's Office of Science under the Scientific Discovery through Advanced Computing (SciDAC), and the Laboratory Directed Research and Development program at Sandia National Laboratories, United States.

References

[1] Caldwell Peter M, Mametjanov Azamat, Tang Qi, Van Roekel Luke P, Golaz Jean-Christophe, Lin Wuyin, et al. The DOE E3SM coupled model version 1: Description and results at high resolution. J Adv Modelling Earth Syst 2019;n/a(n/a).
[2] Piperno Serge, Farhat Charbel. Partitioned procedures for the transient solution of coupled aeroelastic problems – Part II: energy transfer analysis and three-dimensional applications. Comput Methods Appl Mech Engrg 2001;190(24–25):3147–70, Advances in Computational Methods for Fluid-Structure Interaction.
[3] de Boer A, van Zuijlen AH, Bijl H. Review of coupling methods for non-matching meshes. Comput Methods Appl Mech Engrg 2007;196(8):1515–25, Domain Decomposition Methods: recent advances and new challenges in engineering.
[4] Förster Christiane, Wall Wolfgang A, Ramm Ekkehard. Artificial added mass instabilities in sequential staggered coupling of nonlinear structures and incompressible viscous flows. Comput Methods Appl Mech Engrg 2007;196(7):1278–93.
[5] Toth Alex, Kelley CT. Convergence analysis for Anderson acceleration. SIAM J Numer Anal 2015;53(2):805–19.
[6] Banks JW, Henshaw WD, Schwendeman DW, Tang Qi. A stable partitioned FSI algorithm for rigid bodies and incompressible flow. Part I: Model problem analysis. J Comput Phys 2017;343:432–68.
[7] Carey GF, Chow SS, Seager MK. Approximate boundary-flux calculations. Comput Methods Appl Mech Engrg 1985;50(2):107–20.
[8] Peterson Kara, Bochev Pavel, Kuberry Paul. Explicit synchronous partitioned algorithms for interface problems based on Lagrange multipliers. Comput Math Appl 2019;78(2):459–82.
[9] Fairall Chris W, Bradley Edward F, Rogers David P, Edson James Bearer, Young George S. Bulk parameterization of air-sea fluxes for tropical ocean-global atmosphere coupled-ocean atmosphere response experiment. J Geophys Res: Oceans 1996;101(C2):3747–64.
[10] Lemarié Florian, Blayo Eric, Debreu Laurent. Analysis of ocean-atmosphere coupling algorithms: consistency and stability. Procedia Comput Sci 2015;51:2066–75.
[11] Lemarie F, Blayo E, pelletier C, Debreu L. Analysis of ocean-atmosphere coupling algorithms: Consistency and stability. In: Presentation at the 7th international conference on coupled problems. 2017.
[12] Lions Jacques-Louis, Temam Roger, Wang Shouhong. Models of the coupled atmosphere and ocean(CAO I). Comput Mech Adv 1993;1(1):5–54.
[13] Lions JL, Temam R, Wang S. Numerical analysis of the coupled atmosphere-ocean models(CAO II) 0. Comput Mech Adv 1993;1(1):55–119.
[14] Lions Jl L, Temam R, Wang S. Mathematical study of the coupled models of atmosphere and ocean (CAO III). J Math Pures Appl 1995;74:105–63.
[15] Connors Jeffrey M, Howell Jason S, Layton William J. Decoupled time stepping methods for fluid-fluid interaction. SIAM J Numer Anal 2012;50(3):1297–319.
[16] Connors Jeffrey M, Dolan Robert D. Stability of two conservative, high-order fluid-fluid coupling methods. Adv Appl Math Mech 2019;11(6):1287–338.
[17] Zhang Hong, Liu Zhengyu, Constantinescu Emil, Jacob Robert. Stability analysis of interface conditions for ocean-atmosphere coupling. 2019, arXiv preprint arXiv:1909.00916.
[18] Aggul Mustafa, Connors Jeffrey M, Erkmen Dilek, Labovsky Alexander E. A defect-deferred correction method for fluid-fluid interaction. SIAM J Numer Anal 2018;56(4):2484–512.
[19] Connors Jeffrey Mark, Ganis Benjamin. Stability of algorithms for a two domain natural convection problem and observed model uncertainty. Comput Geosci 2011;15(3):509–27.
[20] Javili A, Kaessmair S, Steinmann P. General imperfect interfaces. Comput Methods Appl Mech Engrg 2014;275:76–97.
[21] Brezzi Franco, Douglas Jim. Stabilized mixed methods for the Stokes problem. Numer Math 1988;53:225–35.
[22] Brezzi F. On existence, uniqueness and approximation of saddle-point problems arising from Lagrange multipliers. Model Math Anal Numer 1974;21.
[23] Brezzi F, Fortin M. Mixed and hybrid finite element methods. Berlin: Springer; 1991.
[24] Brezzi Franco, Bathe Klaus-Jurgen. A discourse on the stability conditions for mixed finite element formulations. Comput Methods Appl Mech Engrg 1990;82(1–3):27–57, Proceedings of the Workshop on Reliability in Computational Mechanics.
[25] Gunzburger MD. Finite element methods for viscous incompressible flows. Boston: Academic; 1989.